Field Experiments on Closed-Loop SU-MIMO Transmission Considering Effect of Antenna Configurations in LTE-Advanced Uplink

Shinpei Yasukawa[†], Teruo Kawamura[†], Yoshihisa Kishiyama[†], Hidekazu Taoka[‡], and Hidehiro Andoh[†]

[†]Radio Access Network Development Department,
NTT DOCOMO, INC.
3-5 Hikari-no-oka, Yokosuka-shi, Kanagawa-ken 239-8536 Japan

[‡]DOCOMO Communications Laboratories Europe GmbH
Landsberger Strasse 312, 80687, Munich, Germany

***Abstract*— This paper presents experimental results to clarify the throughput performance and effective location probability for closed-loop single-user (SU)-MIMO transmission considering the effect of antenna configurations in the LTE-Advanced uplink. The achievable throughput performance with adaptive modulation and coding (AMC) and hybrid automatic repeat request (HARQ) is evaluated using the implemented LTE-Advanced transceivers, where the total transmission power and bandwidth per component carrier of a mobile station (MS) are set to 23 dBm and 17.28 MHz, respectively. The experimental results show that when 2-by-2 Rank-2 SU-MIMO, i.e., spatial multiplexing, is applied, a cross-polarized antenna configuration exhibits better throughput performance compared to that using co-polarized antennas and the location probability for achieving throughput greater than 200 Mbps is clearly increased due to the reduction in the inter-stream interference. Furthermore, we confirm that the throughput performance using cross-polarized antennas is very robust against the variation in MS antenna angles irrespective of the rank values for SU-MIMO transmission. The experimental results also show that 2-by-2 Rank-2 SU-MIMO using the cross-polarized antennas improves the throughput performance compared to 1-by-2 SIMO at the location probability of greater than 60% even when the MS antenna gain imbalance level of 12 dB is considered.**

Keywords*— *LTE-Advanced; Single carrier; Single user MIMO; Polarized antenna; Field experiment

I. INTRODUCTION

In the 3rd Generation Partnership Project (3GPP), the radio interface specifications for the next generation mobile communication system called the Long-Term Evolution (LTE) were finalized as LTE Release 8 in 2008 [1],[2]. LTE provides full IP packet-based radio access with low latency and adopts an intra-cell orthogonal multiple access scheme such as orthogonal frequency division multiple access (OFDMA) and single-carrier frequency division multiple access (SC-FDMA) in the downlink and uplink, respectively. In Japan, NTT DOCOMO launched a commercial LTE service in December 2010 under the new service brand of "Xi" (crossy) [3]. Meanwhile, in the 3GPP, standardization efforts towards an enhanced LTE radio interface called LTE-Advanced (LTE Release 10 and beyond) are ongoing [4],[5]. At the beginning of 2011, specifications for LTE Release 10 were finalized, and technical discussions for LTE Release 11 including further radio interface enhancements were initiated.

In the LTE-Advanced uplink, the single-user (SU) multiple-input multiple-output (MIMO) transmission scheme employing codebook based closed-loop transmit diversity with precoding was introduced to as well as the downlink [6],[7]. In this scheme, mobile stations (MSs), i.e., user equipments, periodically transmit a sounding reference signal (SRS) from each transmitter antenna so that the base station (BS) can estimate the uplink MIMO channel responses. Using the estimated MIMO channel responses, the BS determines the rank, i.e., the number of data streams for spatial multiplexing, the precoding vector (PV) for data stream, and the modulation and coding scheme (MCS) for adaptive modulation and coding (AMC) to maximize the expected throughput performance. Finally, the MSs transmit the precoded data stream(s) via the physical uplink shared channel (PUSCH) based on the rank, PV, and MCS values indicated via the downlink control channel.

In [8], we showed the uplink throughput performance with 2-by-2 SU-MIMO and carrier aggregation with two 20-MHz component carriers (CCs) in laboratory experiments using the implemented LTE-Advanced transceiver. The experimental results showed that the peak throughput of approximately 200 Mbps is achieved by applying AMC and hybrid automatic repeat request (HARQ) in multipath fading environments in the uplink. However, the laboratory experiments only assumed fading variation generated by hardware fading simulators under a fixed path loss and shadowing conditions, and the coverage to achieve high throughput performance was not investigated. Therefore, in [9], we presented experimental results that consider a real field environment with considering MS transmission power to clarify the effectiveness of the closed-loop SU-MIMO transmission scheme combined with carrier aggregation in the LTE-Advanced uplink. To the best knowledge of the authors, such field experiments for MIMO transmission techniques with LTE SC-FDMA radio access based on discrete Fourier transform (DFT)-spread OFDM [10] had not been reported.

In this paper, we present further field experimental results on closed-loop SU-MIMO transmission using the SRS for precoding and AMC combined with carrier aggregation in the LTE-Advanced uplink. Since only a fixed antenna configuration employing co-polarized antennas was employed in [9], this paper further evaluates the effect of a cross-polarized antenna configuration and the influence of slanted angles for the MS transmitter antennas considering the antenna gain imbalance. The rest of the paper is organized as follows. In Section II, the principle of the uplink closed-loop SU-MIMO transmission is outlined. After the configuration of the implemented transceiver is described in Section III, the field experimental results are shown in Section IV. Finally, Section V summarizes our conclusions.

II. UPLINK CLOSED-LOOP SU-MIMO TRANSMISSION SCHEME

Figure 1 illustrates the simplified operation of uplink closed-loop SU-MIMO transmission in the implemented LTE-Advanced transceiver. We assume that there are two transmitter and receiver antennas each in the experiments. The MS periodically transmits an SRS, which is used to estimate the MIMO channel for link adaption such as AMC and closed-loop SU-MIMO operations, i.e., closed-loop transmit diversity with precoding. A Zadoff-Chu sequence [11], which is one of the family of constant amplitude zero auto correlation (CAZAC) sequences, is used as the SRS sequence and the SRS symbols from different transmitter antennas are code division multiplexed using different cyclic shifts [12]. At the BS,

978-1-4673-0990-5/12/$31.00 ©2012 IEEE

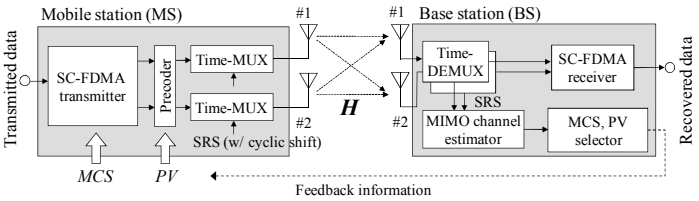

Figure 1. Schematic diagram of uplink closed-loop SU-MIMO transmission.

the MCS used for AMC and PV used for closed-loop transmit diversity with precoding are determined based on the estimated MIMO channel responses using the SRS as explained below. First, the tentative channel gains at each frequency component (subcarrier) for each received antenna are computed by multiplying the received SRS sequence by the conjugate of the SRS sequence replica in the frequency domain. Then, the inverse fast Fourier transform (IFFT) converts the tentative channel gain into the time domain response. By applying the window function in the time domain, noise components at the sample points outside the window are removed. Here, the window length is set to 13.83 μsec so that the delayed paths are included within the window. After the FFT operation, we obtain a frequency domain channel response at each subcarrier position used for MCS and PV selection. Regarding the closed-loop transmit diversity with precoding in the LTE-Advanced uplink, only wideband precoding, i.e., selection of one suitable PV that is common to the contiguously allocated resource blocks (RBs) in the frequency domain within a CC, is adopted in order to avoid an increase in the peak-to-average power ratio (PAPR) due to the frequency selective precoding.

In this paper, the rank value is semi-statically configured. In the case of Rank-2, SU-MIMO multiplexing based on per-antenna rate control (PARC) without precoding is applied. Therefore, PV selection is performed only in the case of Rank-1. Let $\hat{h}_{i,j}^{(k)}$ be the channel estimate at the k-th subcarrier position (k = 1, 2, …, N_S) from the i-th transmitter antenna (i = 1, 2) for the j-th receiver antenna (j = 1, 2). Then, in order to maximize the precoding gain, the optimum PV, $\mathbf{V}_{opt}$, is selected from the codebook, $\mathbf{V}^{(p)} = (v_1^{(p)}, v_2^{(p)})$ $(1 \le p \le P)$, where P represents the codebook size, according to the following equation.

$$\mathbf{V}_{opt} = \arg\max_{p} \left(\frac{1}{N_S} \sum_{k \in \mathbf{S}} \sum_{j=1}^{2} \left| \sum_{i=1}^{2} \hat{h}_{i,j}^{(k)} v_i^{(p)} \right|^2 \right), \quad (1)$$

where $\boldsymbol{S}$ represents sets of subcarrier indices assigned to the PUSCH transmission bandwidth and N_S is the number of elements in $\boldsymbol{S}$. Finally, with the assigned PUSCH transmission bandwidth, the MS transmits the precoded data signal and demodulation reference signal (DM-RS), which is used for channel estimation for coherent demodulation/detection of the data signal.

III. Configuration of Implemented LTE-Advanced Transceiver

The configuration of the implemented LTE-Advanced SC-FDMA transmitter and receiver and the major radio link parameters are given in Fig. 2 and Table I, respectively. We employ 2-by-2 SU-MIMO transmission and carrier aggregation using 2 CCs (each CC has a signal bandwidth of 18 MHz, which is supported in the system bandwidth of 20 MHz in LTE Release 8). Thus, the total signal bandwidth and the number of subcarriers of the SC-FDMA signal are 36 MHz and 2400, respectively (the subcarrier separation is 15 kHz). The subframe duration, i.e., transmission time interval (TTI), is 1 msec, which contains 14 SC-FDMA symbols, each of which comprises 66.67 μsec of effective data and a 4.69 μsec cyclic prefix (CP). Within a subframe, multiple signals and physical channels such as the DM-RS, SRS, and PUSCH are mapped. The two DM-

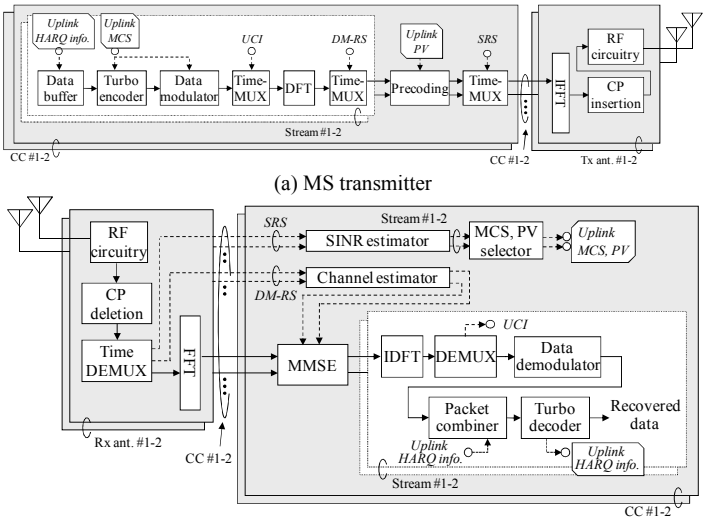

Figure 2. Configuration of implemented LTE-Advanced transceiver with uplink closed-loop SU-MIMO transmission.

TABLE I. Major radio parameters

Carrier frequency		3.67125 GHz
System bandwidth		40 MHz (2 CCs)
Antenna configuration		1-by-2, 2-by-2
Subframe length		1.0 msec
Symbol duration		66.67 μsec
Cyclic prefix duration		4.69 μsec
Channel coding / decoding		Turbo coding / Max-Log-MAP decoding
Receiver		MMSE-based frequency domain equalizer
HARQ	Round trip delay	8 msec
	Max. number of transmissions	3
	Packet combining	Incremental redundancy (IR)
Control delay of AMC, Precoding		8 msec

RS symbols and SRS symbol are time division multiplexed with data symbols at the fourth, eleventh and the last SC-FDMA symbol, respectively, within a subframe. Similar to the SRS sequence, a Zadoff-Chu sequence is also used as the DM-RS sequence. For Rank-1 SU-MIMO, i.e., closed-loop transmit diversity with precoding, the same PV as that for data signals is multiplied to the DM-RS symbols from different transmission antennas. Meanwhile, for Rank-2 SU-MIMO, i.e., SU-MIMO multiplexing, the DM-RS symbols from different transmission antennas are code division multiplexed using different cyclic shifts. The SRS is transmitted with a 96-RB bandwidth (= 17.28 MHz) for each CC irrespective of the transmission bandwidth for the PUSCH. The transmission period for the SRS and the transmission power ratio of the SRS to PUSCH per RB are set to 5 msec and 0 dB, respectively. In the MS transmitter, the information binary data sequence is turbo encoded using the channel coding rate of R with the constraint length of four bits. After channel encoding, data modulation mapping using QPSK, 16QAM, or 64QAM is performed. The modulated data sequence is input to a DFT operation block, where the number of DFT points is equal to the number of subcarriers assigned to the PUSCH. The transmission bandwidth of the PUSCH is set to 96 RBs (= 17.28 MHz) per CC. The data sequence after the DFT operation is mapped to the PUSCH. After applying a 4096-point IFFT, a CP is added at the beginning of each SC-FDMA symbol. After conversion into baseband in-phase (I) and quadrature (Q) components by digital-to-analog (D/A) converters, quadrature-modulation is

performed. Finally, the IF modulated signal is up-converted into the RF signal and amplified by the power amplifier, where the center carrier frequency is 3.67125 GHz. The cross-polarized antennas at the MS comprise a vertically-polarized and horizontally-polarized antenna with the beam pattern of omni-directional in azimuth. The antenna gain of the vertically-polarized and horizontally-polarized antennas is approximately 2 dBi.

At the BS receiver, the received signal is fed into cross-polarized antennas. The cross-polarized antennas at the BS comprise a vertically-polarized and horizontally-polarized antenna using 10-element co-linear antennas with the antenna gain of approximately 18 dBi, respectively. The 3-dB beam width is approximately 90 degrees in azimuth. The RF signal is frequency down-converted into an IF signal and then input into an automatic gain control (AGC) amplifier with the dynamic range of approximately 50 dB. The received signal is converted into baseband I and Q components by a quadrature detector. The I and Q signals are converted into a digital format by 14-bit analog-to-digital (A/D) converters. After the CP is removed, the data sequences are de-multiplexed into each frequency component by a 4096-point FFT. Frequency-domain channel estimation is performed using the DM-RS and SRS. The recovered channel gain is used for the linear minimum mean square error (LMMSE) weight calculation in the frequency domain equalizer. For Rank-2 SU-MIMO, the MMSE signal detection between two-data streams is additionally employed. Finally, after inverse DFT (IDFT) operation, the resultant sequences are turbo decoded using the Max-Log-MAP algorithm using six iterations to recover the transmitted binary data.

Table II and Table III summarize the set of 13 MCSs used for AMC and the set of 6 PVs used for Rank-1 SU-MIMO, respectively, in the experiments. AMC is performed according to the instantaneous measured signal-to-interference plus noise power ratio (SINR) using the SRS. The control delay of the AMC and closed-loop precoding is 8 msec. We use incremental redundancy as the HARQ scheme with packet combining and the round trip delay for retransmission is 8 msec. The feedback control signaling, i.e., MCS, PV, and HARQ-related information, is transmitted via the downlink control channel.

TABLE II. MCS SET FOR AMC

Index	Modulation	Coding rate	Index	Modulation	Coding rate
1	QPSK	0.37	8	16QAM	0.74
2		0.50	9	64QAM	0.55
3		0.62	10		0.62
4	16QAM	0.41	11		0.67
5		0.50	12		0.75
6		0.58	13		0.86
7		0.64			

TABLE III. PV SET FOR 2-BY-2 RANK-1 SU-MIMO

p	1	2	3	4	5	6
$\boldsymbol{V}^{(p)}$	$\frac{1}{\sqrt{2}}\begin{bmatrix}1\\1\end{bmatrix}$	$\frac{1}{\sqrt{2}}\begin{bmatrix}1\\-1\end{bmatrix}$	$\frac{1}{\sqrt{2}}\begin{bmatrix}1\\j\end{bmatrix}$	$\frac{1}{\sqrt{2}}\begin{bmatrix}1\\-j\end{bmatrix}$	$\frac{1}{\sqrt{2}}\begin{bmatrix}1\\0\end{bmatrix}$	$\frac{1}{\sqrt{2}}\begin{bmatrix}0\\1\end{bmatrix}$

IV. FIELD EXPERIMENTS

A. Conditions of Field Experiments

The field experiments were conducted in measurement courses in the YRP district in Yokosuka city near Tokyo, Japan. Fig. 3 shows the measurement courses and the location of the BS transceiver antennas. The heights of the BS cross-polarized antennas are approximately 39.6 m from the ground. The MS cross-polarized antennas are mounted on the top of a measurement vehicle at a height of approximately 3.1 m. The total transmission power of the MS is set to 23 dBm. The measurement vehicle equipped with the

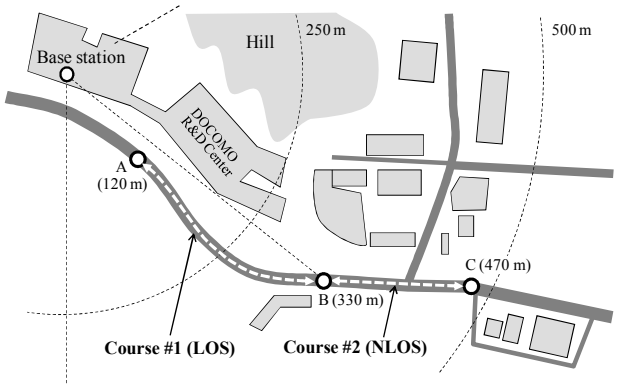

Figure 3. Measurement courses.

MS is driven along Course #1 and Course #2 at the average speed of approximately 10 km/h, where the distance from the BS is approximately 120, 330, and 470 m at points A, B, and C, respectively, in the figure. In Course #1, the BS antennas were in direct line-of-sight (LOS) from the vehicle with MS transceiver. Meanwhile, the majority of Course #2 is under non-LOS (NLOS) conditions due to the surrounding office buildings that are approximately three to six stories high between the transmitter and receiver.

B. Influence of MS Cross-Polarized Antenna Angle on Measured Throughput

Figs. 4(a) and 4(b) show the cumulative distribution functions (CDFs) of the measured received signal strength indicator (RSSI) averaged over 100 msec among transmitter/receiver cross-polarized antennas for a 1-by-1 SISO antenna configuration in Course #1 and Course #2, respectively. In the figures, the MS antenna angle is parameterized at 0, 45, and 90 degrees. Fig. 4(a) shows that when the MS antenna angle is 0 degrees, the measured RSSI values among the vertically-polarized transmitter (V-Tx) / vertically-polarized receiver (V-Rx) or H-Tx / H-Rx antennas along Course #1 under LOS conditions are greater by more than 9 dB at the 50% CDF compared to those among the V-Tx / H-Rx or H-Tx / V-Rx antennas. This is because the power of the direct wave is dominant under LOS conditions and the rotations of vertically and horizontally polarized waves due to the reflections and diffraction against the surrounding buildings are small. In the case of the MS antenna angle of 45 degrees, the figure shows that the difference in such measured RSSI values becomes small due to the rotation of the polarized plane for the MS transmitter antenna. In the case of the MS antenna angle with 90 degrees, the tendency opposite to the case of the MS antenna angle of 0 degrees is observed since the polarized plane for the MS transmitter antenna is interchanged each other. Fig. 4(b) shows that when MS antenna angle is 0 degrees, unlike the LOS conditions the measured RSSI values using the H-Tx antenna are smaller than those using the V-Tx antenna in Course #2 under NLOS conditions. The results indicate that the propagation loss of the transmitted signals from the horizontally-polarized antennas is greater than that from the vertically-polarized antennas as indicated in [13].

Fig. 5 shows the measured throughput distribution performance for 2-by-2 Rank-2 SU-MIMO employing AMC and HARQ as a function of the measured RSSI averaged over 100 msec in Course #1 and Course #2 when the MS cross-polarized antenna angle is 0 degrees. In the figure, the RSSI is defined as the aggregated value for each receiver antenna. For comparison, we also plot the results of the co-polarized transmitter / receiver antennas, i.e., two V-Tx / two V-Rx antennas. Fig. 5 shows that the throughput of the co-polarized antennas in Course #1 is widely distributed compared to that for the cross-polarized antennas for the same RSSI conditions. Furthermore, Fig. 5 shows that 2-by-2 Rank-2 SU-MIMO using the

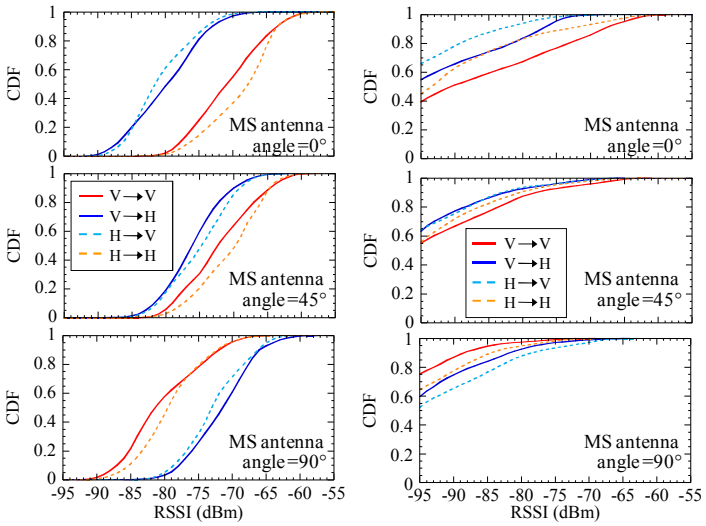

(a) Course #1 (LOS) (b) Course #2 (NLOS)

Figure 4. RSSI among Tx/Rx cross-polarized antennas.

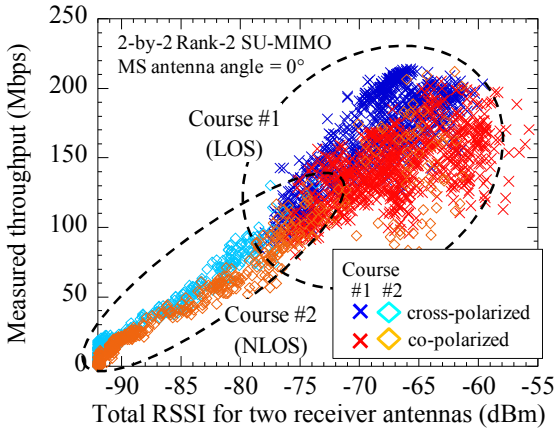

Figure 5. Measured throughput distribution as a function of RSSI.

cross-polarized antennas achieves better throughput performance compared to that using the co-polarized antennas although the average value of the measured RSSI for the co-polarized antennas is larger than that for the cross-polarized antennas in Course #1 and Course #2. This is because the inter-stream interference in MIMO special multiplexing, i.e., the data signals among V-Tx / H-Rx and H-Tx / V-Rx antennas, is significantly reduced by applying cross-polarized antenna configuration as shown in Fig. 4. The merit of the reduction for the inter-stream interference exceeds the demerit of the degradation in the total received signal power by applying the cross-polarized antenna configuration.

In Figs. 6, we present the experimental results for the influence of the slanted angle for the MS cross-polarized transmitter antennas on the measured throughput for 2-by-2 Rank-2 and Rank-1 SU-MIMO. Fig. 6(a) shows the CDFs of the measured throughput performance averaged over 100 msec for 2-by-2 Rank-2 SU-MIMO employing AMC and HARQ over the whole measurement course when the MS cross-polarized antenna angle is parameterized at 0, 45, and 90 degrees. The performance levels for co-polarized antennas when the MS antenna angle is set to 0 and 90 degrees and the 1-by-2 SIMO antenna configuration when the MS antenna angle is ideally set to 0 degrees are also plotted. This figure shows that even when the MS antenna angle is 90 degrees, 2-by-2 Rank-2 SU-MIMO using the cross-polarized antennas effectively improves the throughput performance compared to that using the co-polarized

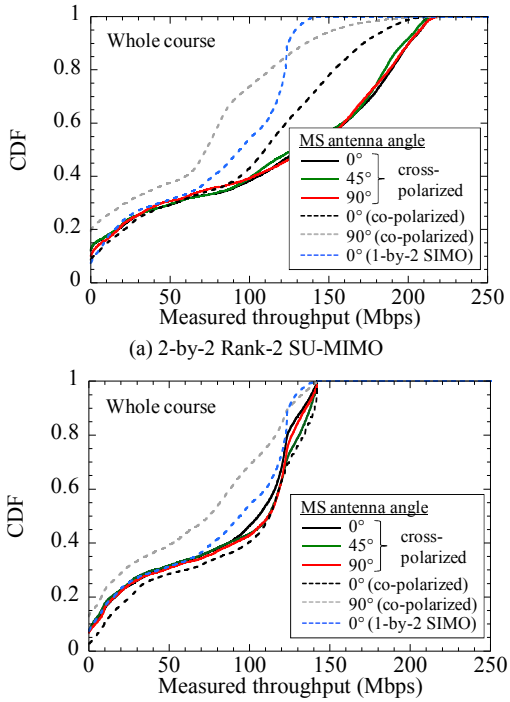

(a) 2-by-2 Rank-2 SU-MIMO

(b) 2-by-2 Rank-1 SU-MIMO

Figure 6. Influence of MS cross-polarized antenna angle.

antennas or 1-by-2 SIMO for the majority of the measurement course except for the low throughput region. Actually, the location probability for achieving throughput greater than 200 Mbps is clearly increased compared to the case using the co-polarized antennas. This figure also shows that almost the same throughput performance levels for cross-polarized antennas are achieved irrespective of the MS antenna angle. By contrast, the throughput performance for co-polarized antennas is severely degraded in the case of the MS antenna angle with 90 degrees compared to that in the case of MS antenna angle with 0 degrees. Fig. 6(b) shows the CDFs of the measured throughput performance averaged over 100 msec for 2-by-2 Rank-1 SU-MIMO employing AMC and HARQ over the whole measurement course when the MS cross-polarized antenna angle is parameterized at 0, 45, and 90 degrees. The performance levels for co-polarized antennas when the MS antenna angle is set to 0 and 90 degrees and the 1-by-2 SIMO antenna configuration when the MS antenna angle is ideally set to 0 degrees are also plotted. This figure shows that when the MS antenna angle is 0 degrees, the throughput performance for 2-by-2 Rank-1 SU-MIMO using the cross-polarized antennas is slightly degraded compared to that using the co-polarized antennas due to the decrease in the total received signal power by applying the cross-polarized antenna configuration. However, it should be noted that when the MS antenna angle is 90 degrees, the performance for co-polarized antennas is significantly degraded. Meanwhile, Fig. 6(b) shows that the fluctuation in the throughput performance due to the variation in the MS antenna angles is not so severe when cross-polarized antennas are used. In this case, slightly better throughput performance is achieved when the MS cross-polarized antenna angle is 45 degrees. This is because the appropriate PV is selected according to the MS cross-polarized antenna angle, and consequently almost a constant received signal power is maintained irrespective of the MS cross-polarized antenna angle. As a result, 2-by-2 Rank-1 SU-MIMO using the cross-polarized antennas improves the throughput performance compared to 1-by-2 SIMO even when the influence of MS cross-polarized antenna angle is considered.

C. Influence of Antenna Gain Imbalance on Measured Throughput

Here, we present the experimental results regarding the influence of the slanted angle for the MS cross-polarized transmitter antennas considering the antenna gain imbalance on the measured throughput for 2-by-2 Rank-2 and Rank-1 SU-MIMO. In the evaluation of the antenna gain imbalance, we assume that the attenuation level of the transmission power for the horizontally-polarized transmitter antenna is parameterized. Fig. 7(a) shows the CDFs of the measured throughput performance averaged over 100 msec for 2-by-2 Rank-2 SU-MIMO employing AMC and HARQ over the whole measurement course when the difference in transmitter antenna gain between the MS cross-polarized antennas is parameterized from 0 to 18 dB. The MS cross-polarized antenna angle is set to 0 degrees. For comparison, the performance levels for 1-by-2 SIMO with the transmission power of 23 and 20 dBm are also plotted. Fig. 7(a) shows that the throughput performance is degraded according to the increase in the imbalance of the antenna gain. For instance, the location probability for achieving throughput greater than 150 Mbps is decreased by approximately 2, 4, 16, and 42% for the antenna gain imbalance level of 3, 6, 12, and 18 dB, respectively, in the measurement course compared to the case without the antenna gain imbalance. However, Fig. 7(a) shows that 2-by-2 Rank-2 SU-MIMO using the cross-polarized antennas improves the throughput performance at the location probability with more than 60% in the measurement course compared to 1-by-2 SIMO even when the antenna gain imbalance level of 12 dB is considered. Fig. 7(b) shows the CDFs of the measured throughput performance averaged over 100 msec for 2-by-2 Rank-1 SU-MIMO employing AMC and HARQ over the whole measurement course when the antenna gain imbalance level is parameterized from 0 to 18 dB. The MS cross-polarized antenna angle is set to 45 degrees. The performance levels for 1-by-2 SIMO with the transmission power of 23 and 20 dBm are also plotted. The figure shows that the throughput performance for 2-by-2 Rank-1 SU-MIMO using the cross-polarized antennas is degraded except in a high throughput region greater than approximately 120 Mbps compared to 1-by-2 SIMO since the total received signal power is decreased due to the antenna gain imbalance in addition to application of the cross-polarized antenna configuration.

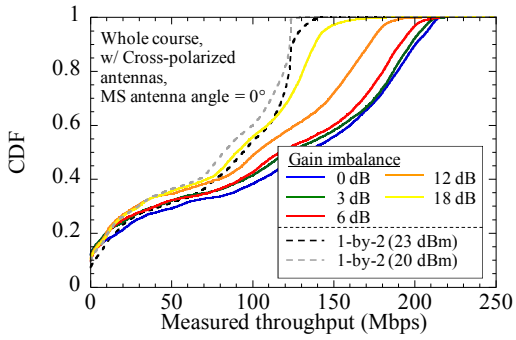

(a) 2-by-2 Rank-2 SU-MIMO

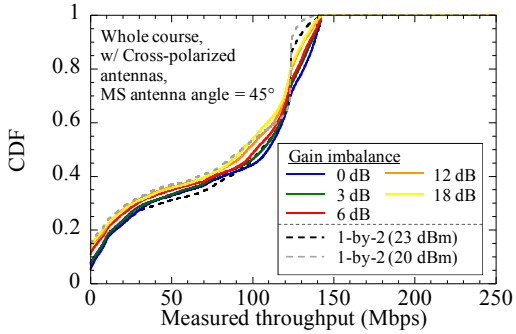

(b) 2-by-2 Rank-1 SU-MIMO

Figure 7. Influence of gain imbalance for MS cross-polarized antennas.

V. Conclusion

This paper presented field experimental results to clarify the throughput performance and effective location probability for closed-loop SU-MIMO transmission considering the effect of antenna configurations in the LTE-Advanced uplink. The achievable throughput performance with AMC and HARQ was evaluated using the implemented LTE-Advanced transceivers, where the total MS transmission power and bandwidth per CC are set to 23 dBm and 96 RBs (= 17.28 MHz), respectively. The experimental results showed that when 2-by-2 Rank-2 SU-MIMO, i.e., spatial multiplexing, is applied, the cross-polarized antenna configuration exhibits better throughput performance compared to that using co-polarized antennas and the location probability for achieving throughput greater than 200 Mbps is clearly increased due to the reduction in the inter-stream interference. Furthermore, we confirmed that throughput performance using cross-polarized antennas is relatively robust against the variation in MS antenna angles irrespective of the rank values for SU-MIMO transmission. The experimental results also showed that 2-by-2 Rank-2 SU-MIMO using the cross-polarized antennas improves the throughput performance compared to 1-by-2 SIMO at the location probability of greater than 60% even when the MS antenna gain imbalance level of 12 dB is considered.

References

[1] 3GPP, TS 36.300 (V8.12.0), "Evolved Universal Terrestrial Radio Access (E-UTRA) and Evolved Universal Terrestrial Radio Access Network (E-UTRAN); Overall description," Apr. 2010.

[2] M. Tanno, Y. Kishiyama, N. Miki, K. Higuchi, and M. Sawahashi, "Evolved UTRA - physical layer overview," *Proc. IEEE SPAWC 2007*, June 2007.

[3] http://www.nttdocomo.com/pr/2010/001494.html

[4] 3GPP, TS 36.201 (V10.0.0), "Evolved Universal Terrestrial Radio Access (E-UTRA); LTE physical layer; General description (Release 10)," Dec. 2010.

[5] E. Dahlman, S. Parkvall, and J. Sköld, 4G –LTE/LTE-Advanced for Mobile Broadband, Academic Press, 2011.

[6] Y. Kakishima, T. Kawamura, H. Taoka, and T. Nakamura, "Suboptimal precoding vector selection scheme combined with frequency domain scheduling for closed-loop MIMO transmission in LTE-Advanced uplink," Proc. IEEE PIMRC 2010, Sep. 2010.

[7] Y. Kakishima, T. Kawamura, H. Taoka, and T. Nakamura, "Evaluation of two-antenna transmit diversity schemes for uplink shared data channel considering channel estimation error in LTE-Advanced," Proc. WPMC 2010, Oct. 2010.

[8] S. Yasukawa, T. Kawamura, Y. Kishiyama, H. Taoka, and T. Nakamura, "Experimental evaluation on SU-MIMO transmission with closed-loop precoding in LTE-Advanced uplink," Proc. IEEE VTC 2011-Spring, May 2011.

[9] S. Yasukawa, T. Kawamura, Y. Kishiyama, H. Taoka, and T. Nakamura, "Experiments on throughput and coverage for closed-loop SU-MIMO transmission combined with carrier aggregation in LTE-Advanced uplink," Proc. IEEE APWCS2011, Aug. 2011.

[10] D. Falconer, S. L. Ariyavisitakul, A. Benyamin-Seeyar, and B. Eidson, "Frequency domain equalization for single-carrier broadband wireless access," IEEE Commun. Mag., vol. 40, no. 4, pp. 58-66, Apr. 2002.

[11] D. C. Chu, "Polyphase codes with good periodic correlation properties," IEEE Trans. Inform. Theory, vol. 18, pp. 531-532, July 1972.

[12] 3GPP, TS 36.211 (V10.2.0), "Evolved Universal Terrestrial Radio Access (E-UTRA); Physical channels and modulation," June 2011.

[13] R.G. Vaughan, "Polarization diversity in mobile communications," IEEE Trans. Veh. Tech. vol. 39, no. 3, pp. 177-186, Aug. 1990.